Electro-osmotic flow through a thin channel with gradually varying wall potential and hydrodynamic slippage

Chiu-On Ng,[1] Qi Zhou

Department of Mechanical Engineering, The University of Hong Kong,
Pokfulam Road, Hong Kong

November 30, 2012

Abstract

The lubrication approximation is applied to electro-osmotic flow through a thin parallel-plate channel under the combined effect of charge and hydrodynamic slippage modulation on the walls. The walls are periodically patterned for the charge and slip distributions, with a wavelength much longer than the channel height. It is shown that the phase of the wall patterns will play a significant role in determining the section-averaged velocity as well as the local convection pattern, quantitatively and qualitatively. The effect of the phase on the flow will be dramatically different, depending on whether the electric field is applied along or perpendicular to the varying direction of the patterns. The possibility of generating a net flow in a direction perpendicular to the applied field is demonstrated.

Keywords: Electro-osmotic flow; boundary slip; lubrication approximation.

[1]Corresponding author. Tel: (852) 2859 2622; Fax: (852) 2858 5415; E-mail address: cong@hku.hk (C.-O. Ng).

1 Introduction

Electro-osmotic (EO) flow through a prismatic channel with homogeneous surface properties is characterized by a nearly uniform or plug-like velocity profile, by which Taylor dispersion will be largely diminished. This is desirable in separation processes, but becomes a disadvantage when mixing is wanted to happen with the flow. Surface inhomogeneity (e.g. topography patterning and charge modulation) can be utilized to generate a vortical flow structure, which helps achieve mixing in a flow driven by electrokinetics (Chang and Yang 2007).

Zeta potential, or the electric potential at the shear plane in the electric double layer formed in the vicinity of a charged wall, may vary spatially by design or owing to unavoidable surface defects. Anderson and Idol (1985) pioneered an analytical study on EO flow in a circular capillary, on the wall of which the zeta potential may vary arbitrarily with axial position. They showed that nonuniformly charged walls can give rise to secondary flow in the form of flow separation and recirculation. Flow perturbations due to such secondary flow structures on dispersion in capillary electrophoresis have been investigated by Long *et al* (1999). Experiments were performed by Herr *et al* (2000) and Stroock *et al* (2000) to compare with theories for EO flow in microchannels with nonuniform zeta potential. Considering a striped pattern of surface charge of alternating sign, Stroock *et al* (2000) demonstrated that various flow types (multidirectional flow or cellular flow) can be generated, depending on whether the applied field is parallel or perpendicular to the stripes.

Ajdari (1995, 1996) took it further to look into superposition of periodic surface charge and topography patterns. For flow between two parallel plates, Ajdari showed that the combined effect of charge and shape modulation on the surfaces is to generate net flow and force on the plates even if the plates are on average electro-neutral. Charge modulation alone can only give rise to periodic convective rolls, but is unable to generate net flow. Net effects can happen when the symmetry of flow induced by positive–negative charges is broken by the superposition of an undulated wall. The net flow can be in a direction as if it were uniformly negatively charged even when the average wall charge is positive, and vice versa. As a result, under the combined effect of charge modulation and

surface undulation, it is possible to generate a flow that is strictly perpendicular to the applied field in some well-chosen configurations. For channels of arbitrary cross-section and wall charge distribution, Ghosal (2002) applied the lubrication theory to EO flow in channels where the cross-section and surface charge vary slowly in the axial direction.

Surface inhomogeneity may cause hydrodynamic slippage to vary spatially as well. Squires (2008) developed some general relations, in the thin double-layer limit, for electrokinetic flows over a surface exhibiting heterogeneous distributions of slip length and zeta potential. The problem of EO flow over an inhomogeneously charged and slipping anisotropic superhydrophobic surface was further studied by Belyaev and Vinogradova (2011), who developed relations between EO mobility and hydrodynamic slip under the limiting conditions of a very thin double layer and a very thick channel. The relations were recently generalized by Ng and Chu (2011), who derived Onsager relations for electro-hydrodynamic flow through a planar channel made up of stripe-patterned superhydrophobic surfaces, where the channel and the electric double layer can be of arbitrary thickness.

One may interpret slip length as the distance into the envelope of a surface where the velocity profile extrapolates to zero. In other words, the no-slip plane is shifted outward. Therefore, flow over a surface with a finite slip length is in some sense equivalent to flow over a no-slip but outwardly displaced surface. This explains why the combined effect of charge and shape modulation (Ajdari 1996) is in many ways similar to the combined effect of charge and hydrodynamic slip modulation (Belyaev and Vinogradova 2011). In the former, it is an undulated surface, while in the latter, it is a nonuniform slip length distribution, which breaks the symmetry of flow induced by a balanced positive–negative charge distribution. Belyaev and Vinogradova (2011) have demonstrated that it is possible to generate an EO flow over a superhydrophobic surface in a direction as if the surface were uniformly negatively charged despite an average positive charge of the surface. This flow behavior is similar to that found by Ajdari (1996), but the flow can be altered by the hydrodynamic effective slip more dramatically than by the shape modulation on the surface.

As suggested by Vinogradova and Belyaev (2011), it is of interest to consider EO flow through a thin gap bounded by superhydrophobic surfaces with spatially varying

partial slip. This has motivated the present study. In this paper, we solve for the EO velocity field in a long and narrow parallel-plate channel under the condition that the zeta potential and the hydrodynamic slip on the surface of the two plates vary slowly in a direction parallel or perpendicular to the applied field. The gap bounded by the surfaces is so thin that the lubrication approximation can be applied, but is not so thin that the electric double layers overlap. The slip length is of the same length scale as the channel height, which is much smaller than the length scale for variations in the direction of charge and slip modulation on the walls. The sharp contrast in length scales enables the application of the lubrication theory to the present problem.

An additional parameter, namely the phase, will become influential when flow between two closely-spaced patterned walls is considered. One of our objectives here is to look into how the phase difference of the wall patterns may affect electrokinetic flow through a narrow plane channel with periodic charge and hydrodynamic slip variations on its two walls. Our problem is described in further detail in Section II, where we derive expressions for the EO velocity driven by a field applied in a direction along or perpendicular to the wave of the modulation. Results are then discussed in Section III, where we demonstrate the different behaviors exhibited by the EO mobility, depending on the field direction, interaction between the charge and hydrodynamic slip distributions, and the phase difference of the wall patterns.

2 Analysis by lubrication approximation

We consider electro-osmotic (EO) flow through a narrow plane channel bounded by two very wide and long parallel plates, which are patterned with a micro-structure such that the charge density and the hydrodynamic slip length vary periodically on the plate surfaces. Figure 1 shows a definition sketch of our problem, where the walls are periodically modulated along the direction x and invariant along the direction z. The wall potential and slippage are periodic functions of x, where the wavelength of one periodic unit is L. The y-axis is perpendicular to the two plates which are at a distance h apart. We assume that the wavelength L, which is the length scale for variations in the x-direction, is much longer than the channel height, h, which is the length scale for

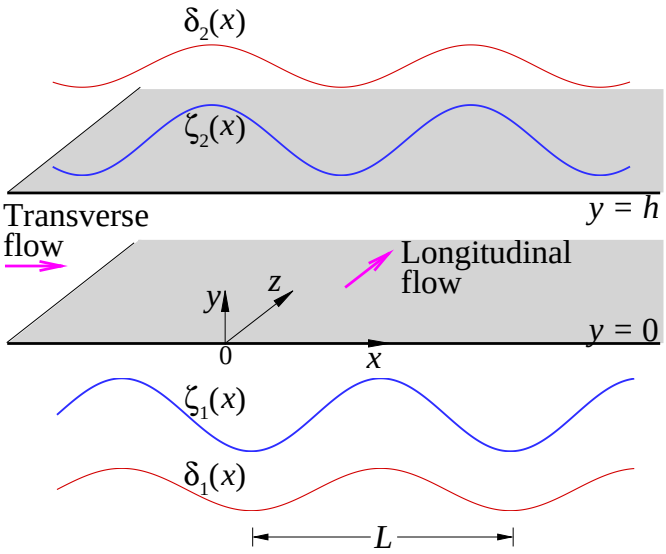

Figure 1: Definition sketch of the problem. The walls are periodically modulated; the zeta potential ζ and the hydrodynamic slip length δ vary slowly along the direction x, but are invariant along the direction z (normal to the $x-y$ plane). Transverse or longitudinal flow occurs when the field is applied along the x-axis, or along the z-axis, respectively. The wavelength is much longer than the channel height: $L \gg h$.

variations in the y-direction. The sharp contrast in the length scales, i.e. $\varepsilon \equiv h/L \ll 1$, implies that the rate of change is much slower in the x-direction than in the y-direction. We further assume that the Reynolds number Re is so small that $\varepsilon \mathrm{Re} \ll 1$, where $\mathrm{Re} = Uh/\nu$, in which U is the scale of the axial velocity and ν is the fluid kinematic viscosity. These two conditions of smallness, one geometric and one dynamic, are the basic requirements for the lubrication approximation. Under these conditions, the flow is nearly unidirectional as the velocity components are in a ratio scaled by ε. In the momentum equations, the inertia terms as well as the derivatives with respect to x are subdominant and can be omitted to a first approximation. The shallowness of the flow also implies that the pressure is locally uniform across the channel.

For sufficiently low wall potentials and non-overlapped electric double layers, the linearized Poisson–Boltzmann equation for the electric potential $\psi(x, y)$ of a symmetric binary electrolyte reads, under the conditions of the lubrication approximation,

$$\frac{\partial^2 \psi}{\partial y^2} = \kappa^2 \psi, \tag{1}$$

where κ is the Debye–Hückel parameter, or the inverse of the Debye length (a measure of the thickness of the electric double layer). Subject to the boundary conditions $\psi = \zeta_1(x)$ at the lower wall $y = 0$, and $\psi = \zeta_2(x)$ at the upper wall $y = h$, the potential can be readily found to be

$$\psi(x, y) = \zeta_1(x)\cosh(\kappa y) + \left[\frac{\zeta_2(x) - \zeta_1(x)\cosh(\kappa h)}{\sinh(\kappa h)}\right]\sinh(\kappa y). \tag{2}$$

The solution is valid for any wall zeta potentials ζ_1 and ζ_2 that are slow functions of x. We leave them unspecified for the time being.

2.1 Transverse flow

Flows in the two principal directions are considered. We first examine transverse flow, which is driven by an electric field E_x along the modulation direction x. The axial velocity being normal to the wall patterns, the flow is nearly unidirectional in the x-direction. The approximate x-momentum equation reads

$$\frac{\partial^2 u}{\partial y^2} = \frac{1}{\mu}\frac{\partial p'}{\partial x} + \frac{\epsilon\kappa^2 E_x}{\mu}\psi, \tag{3}$$

where $u(x, y)$ is the x-component velocity, μ is the fluid dynamic viscosity, ϵ is the dielectric constant of the electrolyte, and $p'(x) = p - \epsilon\kappa^2\psi^2/2$ is the effective pressure (the electrostatic pressure being subtracted from the pressure p).

The flow is subject to Navier's slip boundary condition at the two walls:

$$u = \delta_1(x)\frac{\partial u}{\partial y} \qquad \text{at } y = 0, \tag{4}$$

$$u = -\delta_2(x)\frac{\partial u}{\partial y} \qquad \text{at } y = h, \tag{5}$$

where $\delta_1(x)$ and $\delta_2(x)$ are respectively the hydrodynamic slip lengths at the lower and upper walls. They can be any slow functions of x. We also leave them unspecified for the time being. After some algebra on solving equations (3)–(5), the axial velocity is found as follows:

$$\begin{aligned} u(x, y) \;=\; & -\frac{\partial p'}{\partial x}\frac{h^2}{2\mu}\left[-\frac{y^2}{h^2} + \left(\frac{h + 2\delta_2(x)}{F(x)}\right)\left(\frac{y}{h} + \frac{\delta_1(x)}{h}\right)\right] \\ & - \frac{\epsilon E_x}{\mu}\left[-\zeta_1(x)\cosh(\kappa y) + \left(\frac{\zeta_1(x)}{\tanh(\kappa h)} - \frac{\zeta_2(x)}{\sinh(\kappa h)}\right)\sinh(\kappa y)\right. \end{aligned}$$

$$
\begin{aligned}
&+\frac{h\zeta_1(x)+\delta_1(x)\zeta_2(x)+\delta_2(x)\zeta_1(x)-(\zeta_1(x)-\zeta_2(x))\,y}{F(x)}\\
&-\left(\frac{\delta_1(x)\zeta_1(x)-\delta_2(x)\zeta_2(x)}{\tanh(\kappa h)}+\frac{\delta_2(x)\zeta_1(x)-\delta_1(x)\zeta_2(x)}{\sinh(\kappa h)}\right)\frac{\kappa y}{F(x)}\\
&+\left(\frac{h\zeta_1(x)+\delta_2(x)\zeta_1(x)+\delta_2(x)\zeta_2(x)}{\tanh(\kappa h)}\right.\\
&\left.-\frac{h\zeta_2(x)+\delta_2(x)\zeta_1(x)+\delta_2(x)\zeta_2(x)}{\sinh(\kappa h)}\right)\frac{\kappa\delta_1(x)}{F(x)}\Bigg],
\end{aligned}
\tag{6}
$$

where $F(x)=h+\delta_1(x)+\delta_2(x)$.

Let us introduce the following normalization, in which the normalized quantities are distinguished by an overhead caret:

$$
\hat{x}=x/L,\quad (\hat{y},\,\hat{\delta})=(y,\,\delta)/h,\quad \hat{\kappa}=\kappa h,\quad \hat{\zeta}=\zeta/\zeta_0,
\tag{7}
$$

where ζ_0 is a scale for the wall potential (typically 25 mV at room temperature for a binary electrolyte). On averaging across the section, the section-mean EO velocity is given by

$$
\bar{u}=\int_0^1 u\,d\hat{y}=A(\hat{x})P_x^*(\hat{x})+B(\hat{x})E_x^*,
\tag{8}
$$

where

$$
P_x^*(\hat{x})=-\frac{h^2}{\mu}\frac{\partial p'}{\partial x},\qquad E_x^*=-\frac{\epsilon\zeta_0}{\mu}E_x
\tag{9}
$$

are quantities with dimensions of velocity, and

$$
A(\hat{x})=-\frac{1}{6}+\frac{\left(1+2\hat{\delta}_1(\hat{x})\right)\left(1+2\hat{\delta}_2(\hat{x})\right)}{4\hat{F}(\hat{x})},
\tag{10}
$$

$$
\begin{aligned}
B(\hat{x}) \;=\; &-\left(\hat{\zeta}_1(\hat{x})+\hat{\zeta}_2(\hat{x})\right)\left(\frac{\cosh(\hat{\kappa})-1}{\hat{\kappa}\sinh(\hat{\kappa})}\right)\\
&+\frac{\hat{\zeta}_1(\hat{x})+\hat{\zeta}_2(\hat{x})+2\hat{\delta}_1(\hat{x})\hat{\zeta}_2(\hat{x})+2\hat{\delta}_2(\hat{x})\hat{\zeta}_1(\hat{x})}{2\hat{F}(\hat{x})}\\
&+\frac{\hat{\kappa}\left(\hat{\delta}_1(\hat{x})\hat{\zeta}_1(\hat{x})+\hat{\delta}_2(\hat{x})\hat{\zeta}_2(\hat{x})\right)+2\hat{\kappa}\hat{\delta}_1(\hat{x})\hat{\delta}_2(\hat{x})\left(\hat{\zeta}_1(\hat{x})+\hat{\zeta}_2(\hat{x})\right)}{2\hat{F}(\hat{x})\tanh(\hat{\kappa})}\\
&-\frac{\hat{\kappa}\left(\hat{\delta}_1(\hat{x})\hat{\zeta}_2(\hat{x})+\hat{\delta}_2(\hat{x})\hat{\zeta}_1(\hat{x})\right)+2\hat{\kappa}\hat{\delta}_1(\hat{x})\hat{\delta}_2(\hat{x})\left(\hat{\zeta}_1(\hat{x})+\hat{\zeta}_2(\hat{x})\right)}{2\hat{F}(\hat{x})\sinh(\hat{\kappa})},
\end{aligned}
\tag{11}
$$

in which $\hat{F}(\hat{x})=1+\hat{\delta}_1(\hat{x})+\hat{\delta}_2(\hat{x})$.

By continuity, the section-mean velocity $\bar{u}$ is independent of the axial coordinate $\hat{x}$. On rearranging equation (8),

$$
P_x^*(\hat{x})=\frac{\bar{u}}{A(\hat{x})}-\frac{B(\hat{x})}{A(\hat{x})}E_x^*.
\tag{12}
$$

In the absence of an externally applied pressure gradient, the pressure drop across one periodic unit is zero, or $\int_0^1 P_x^*(\hat{x})d\hat{x} = 0$, which implies, since E_x^* is a constant,

$$\bar{u} = M_\perp E_x^* \tag{13}$$

where

$$M_\perp = \frac{\int_0^1 B(\hat{x})/A(\hat{x})d\hat{x}}{\int_0^1 1/A(\hat{x})d\hat{x}} \tag{14}$$

is the EO mobility for flow transverse to the wall patterns, as induced by a field applied along the modulation direction x. Putting equation (13) back to equation (12), the induced pressure gradient is

$$P_x^*(\hat{x}) = \left(\frac{M_\perp}{A(\hat{x})} - \frac{B(\hat{x})}{A(\hat{x})}\right) E_x^*. \tag{15}$$

When slightly modified, the present formulation also allows us to determine the hydrodynamic effective slip length for pressure-driven flow through the channel. On setting $E_x^* = 0$ and with the condition that $\int_0^1 P_x^*(\hat{x})d\hat{x} = Kh^2/\mu$ where $K = -(\partial p/\partial x)_{\text{app}}$ is the applied pressure gradient, the analysis above will give the section-mean velocity for pressure-driven flow instead:

$$\bar{u} = \left[\int_0^1 \frac{1}{A(\hat{x})}d\hat{x}\right]^{-1} \frac{Kh^2}{\mu}, \tag{16}$$

by which the hydrodynamic effective slip length for transverse flow can be deduced as

$$\hat{\delta}_{\text{eff}}^{\perp} = 2\left[\int_0^1 \frac{1}{A(\hat{x})}d\hat{x}\right]^{-1} - \frac{1}{6}. \tag{17}$$

Here, effective slip length is the uniform slip length of a channel of the same geometry but with homogeneous walls giving rise to the same discharge under the same hydrodynamic forcing as in the channel with heterogeneous walls under consideration. One can readily check from equation (17) that the effective slip is simply $\hat{\delta}_{\text{eff}}^{\perp} = \hat{\delta}$ if the two slip functions $\hat{\delta}_1 = \hat{\delta}_2 = \hat{\delta} =$ constant.

2.2 Longitudinal flow

We next examine flow that is driven by an electric field E_z in the z-direction, which is perpendicular to the $x - y$ plane shown in figure 1. The flow is exactly unidirectional in the z-direction and is parallel to the wall patterns. No pressure is induced in the flow.

Similar approximation analysis can be performed, resulting in a velocity profile equal to that given in equation (6) without the pressure gradient term:

$$\begin{aligned} w(x,y) &= -\frac{\epsilon E_z}{\mu}\left[-\zeta_1(x)\cosh(\kappa y)+\left(\frac{\zeta_1(x)}{\tanh(\kappa h)}-\frac{\zeta_2(x)}{\sinh(\kappa h)}\right)\sinh(\kappa y)\right. \\ &\quad + \frac{h\zeta_1(x)+\delta_1(x)\zeta_2(x)+\delta_2(x)\zeta_1(x)-(\zeta_1(x)-\zeta_2(x))\,y}{F(x)} \\ &\quad - \left(\frac{\delta_1(x)\zeta_1(x)-\delta_2(x)\zeta_2(x)}{\tanh(\kappa h)}+\frac{\delta_2(x)\zeta_1(x)-\delta_1(x)\zeta_2(x)}{\sinh(\kappa h)}\right)\frac{\kappa y}{F(x)} \\ &\quad + \left(\frac{h\zeta_1(x)+\delta_2(x)\zeta_1(x)+\delta_2(x)\zeta_2(x)}{\tanh(\kappa h)}\right. \\ &\quad \left.\left. -\frac{h\zeta_2(x)+\delta_2(x)\zeta_1(x)+\delta_2(x)\zeta_2(x)}{\sinh(\kappa h)}\right)\frac{\kappa\delta_1(x)}{F(x)}\right], \end{aligned} \tag{18}$$

where $F(x) = h + \delta_1(x) + \delta_2(x)$. The section-mean velocity is therefore

$$\bar{w} = \int_0^1\int_0^1 w d\hat{y} d\hat{x} = M_{\parallel} E_z^*, \tag{19}$$

where $E_z^* = -\left(\epsilon\zeta_0/\mu\right) E_z$ is a constant, and

$$M_{\parallel} = \int_0^1 B(\hat{x}) d\hat{x} \tag{20}$$

is the EO mobility for flow parallel to the wall patterns, in which $B(\hat{x})$ is given by equation (11).

The hydrodynamic effective slip length for pressure-driven longitudinal flow can be deduced in a similar manner. It is

$$\hat{\delta}_{\text{eff}}^{\parallel} = 2\int_0^1 A(\hat{x}) d\hat{x} - \frac{1}{6}, \tag{21}$$

where $A(\hat{x})$ is given in equation (10). Also, one can readily check from equation (21) that the effective slip is simply $\hat{\delta}_{\text{eff}}^{\parallel} = \hat{\delta}$ if the two slip functions $\hat{\delta}_1 = \hat{\delta}_2 = \hat{\delta} =$ constant.

3 Discussion

Let us assume that the walls are sinusoidally modulated with the same wavelength and amplitude, but there can be a phase shift between the two waves. The following sinusoidal functions for the slip lengths and the wall potentials are introduced:

$$\hat{\delta}_1(\hat{x}) = \hat{\delta}_0\left[1+\cos(2\pi\hat{x})\right], \tag{22}$$

$$\hat{\delta}_2(\hat{x}) = \hat{\delta}_0 \left[1 + \cos(2\pi\hat{x} + \phi)\right], \tag{23}$$

$$\hat{\zeta}_1(\hat{x}) = a + b\cos(2\pi\hat{x}), \tag{24}$$

$$\hat{\zeta}_2(\hat{x}) = a + b\cos(2\pi\hat{x} + \phi). \tag{25}$$

In these expressions, $\hat{\delta}_0$ and a are the average values (i.e. the steady components) for the slip length and potential of the walls, respectively, and b is the amplitude of the wavy modulation component of the wall potential. The phase ϕ is the phase lag of the upper wall pattern relative to the lower wall pattern. Here, we have for simplicity assumed that on the same wall the slip length and the potential are in phase with each other. In reality, this is not an unreasonable assumption. For example, the maximum slip (e.g. over a gas bubble) often happens where the potential is the minimum.

For validity of the lubrication approximation, we require that $\hat{\delta}_0$, a and b must not exceed order unity. The slip length varies between the maximum value of $2\delta_0$ and the minimum value of zero. Negative slip length is not considered here. The wall potential, however, may be positive or negative (a positive/negative normalized potential $\hat{\zeta}$ means that the potential ζ is of the same/opposite sign as the reference potential ζ_0). A value of $\hat{\kappa} = 10$ for the Debye–Hückel parameter is used in all the cases discussed below.

3.1 No-slip walls

When the walls are non-slipping, i.e. $\hat{\delta}_0 = 0$, the functions A and B reduce to

$$A = \frac{1}{12}, \qquad B(\hat{x}) = \left(\frac{\hat{\zeta}_1(\hat{x}) + \hat{\zeta}_2(\hat{x})}{2}\right)\left[1 - \frac{\tanh(\hat{\kappa}/2)}{\hat{\kappa}/2}\right]. \tag{26}$$

As A becomes a constant, the two mobilities are equal to each other, and given by

$$M_{\parallel,\perp} = a\left[1 - \frac{\tanh(\hat{\kappa}/2)}{\hat{\kappa}/2}\right]. \tag{27}$$

Hence, in the absence of slippage, the section-averaged flow will be isotropic, despite anisotropy in the distribution of wall potentials. The wavy modulation component of the wall potentials will have no effect on the EO mobility when there is no hydrodynamic slip. The local secondary flow structure is of course always anisotropic, as is affected by the charge modulation on the walls, which is direction dependent (Stroock *et al* 2000).

3.2 Effective slip lengths and the phase

When the wall patterns are in phase, i.e. $\phi = 0$ and $\hat{\delta}_1 = \hat{\delta}_2 = \hat{\delta}_0(1 + \cos 2\pi\hat{x})$, the hydrodynamic effective slip lengths can be analytically obtained from equations (17) and (21) as follows:

$$\hat{\delta}^{\parallel}_{\text{eff}} = \hat{\delta}_0, \qquad \hat{\delta}^{\perp}_{\text{eff}} = \frac{1}{6}\left(\sqrt{1 + 12\hat{\delta}_0} - 1\right) \qquad \text{for } \phi = 0. \tag{28}$$

When the wall patterns are out of phase by half a period, i.e. $\phi = \pi$ and $\hat{\delta}_2 = \hat{\delta}_0(1 - \cos 2\pi\hat{x})$, the effective slip lengths can also be analytically deduced. They are

$$\hat{\delta}^{\parallel}_{\text{eff}} = \frac{\hat{\delta}_0\left(1 + \hat{\delta}_0\right)}{1 + 2\hat{\delta}_0}, \quad \hat{\delta}^{\perp}_{\text{eff}} = \frac{1}{6}\left(\sqrt{\frac{\left(1 + 6\hat{\delta}_0\right)\left(1 + 8\hat{\delta}_0\right)}{1 + 2\hat{\delta}_0}} - 1\right) \qquad \text{for } \phi = \pi. \tag{29}$$

From these analytical results, one can readily show that

$$\hat{\delta}_0 = \hat{\delta}^{\parallel}_{\text{eff}}(\phi = 0) > \hat{\delta}^{\parallel}_{\text{eff}}(\phi = \pi), \tag{30}$$

but

$$\hat{\delta}^{\perp}_{\text{eff}}(\phi = 0) < \hat{\delta}^{\perp}_{\text{eff}}(\phi = \pi) < \hat{\delta}_0. \tag{31}$$

One can further numerically check that $\hat{\delta}^{\parallel}_{\text{eff}}$ is the maximum when $\phi = 0$, and is the minimum when $\phi = \pi$. The opposite is true for $\hat{\delta}^{\perp}_{\text{eff}}$. This finding concurs with that of Wang (1976, 1979) and Ng and Wang (2010), who found that the resistance to flow between two corrugated plates depends on the flow direction as well as on the phase of the corrugations. Slip length is the distance by which the no-slip plane is shifted outward from the physical wall. Therefore, a wall with velocity slip amounts in some sense to a widened channel section. Flow past a wall with variable slip length is comparable to flow past a corrugated wall. When the slip patterns are in phase, the overall drag is the minimum for longitudinal flow, but is the maximum for transverse flow. The opposite is true when the phase of the smallest resistance of one wall meets the phase of the largest resistance of the other wall (i.e. the patterns are half-period out of phase). It is also noteworthy that, except the special case $\hat{\delta}^{\parallel}_{\text{eff}}(\phi = 0) = \hat{\delta}_0$, the effective slip length, for any flow direction and for any phase, is always smaller than the average slip length of the walls.

3.3 Uniform wall potentials

When the walls are uniformly charged, i.e. $b = 0$ and $\hat{\zeta}_1 = \hat{\zeta}_2 = a = 1$, we get from equations (10) and (11)

$$B(\hat{x}) = 1 + \hat{\kappa}\left(2A(\hat{x}) - \frac{1}{6}\right)\tanh(\hat{\kappa}/2) - \frac{\tanh(\hat{\kappa}/2)}{\hat{\kappa}/2}. \tag{32}$$

We then obtain from equations (14), (17), (20) and (21) the mobilities as follows:

$$M_{\parallel,\perp} = 1 + \hat{\kappa}\hat{\delta}_{\text{eff}}^{\parallel,\perp}\tanh(\hat{\kappa}/2) - \frac{\tanh(\hat{\kappa}/2)}{\hat{\kappa}/2}, \tag{33}$$

which is a formula in agreement with the one recently deduced by Ng and Chu (2011) for EO flow through a parallel-plate channel with slipping stripes on walls. Squires (2008) was the first to point out that EO flow over an arbitrarily slipping surface with a constant wall potential is enhanced by precisely the same amount as would be found by naively assuming the effective slip length to apply homogeneously. For any flow direction, the hydrodynamic effective slip length can be used directly in the electrokinetic problem as if the slip were homogeneous (i.e. with a constant slip length equal to the macroscopic effective slip length), as long as the wall potential is constant.

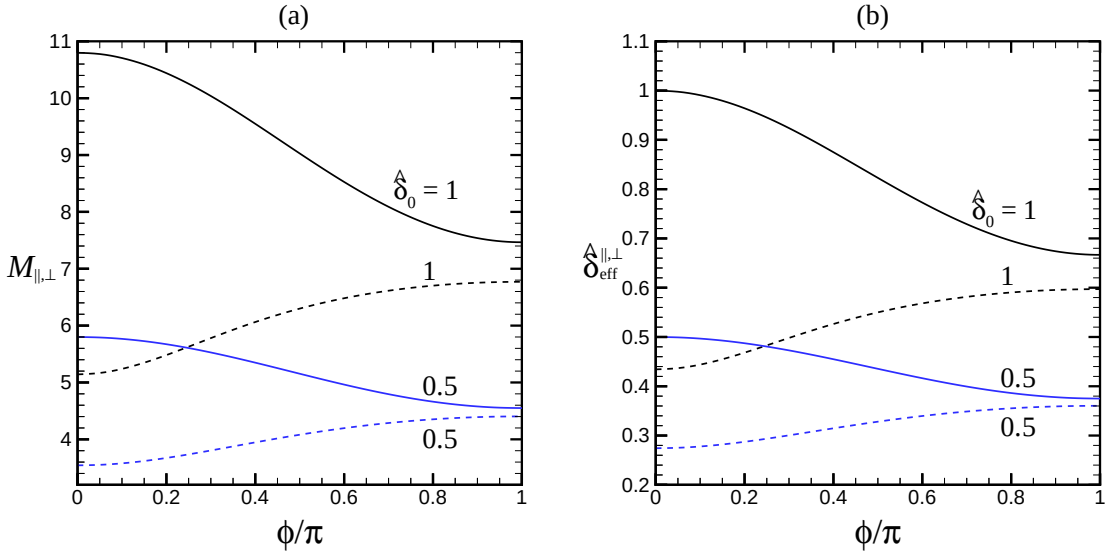

Figure 2: For uniformly charged walls ($a = 1$, $b = 0$, $\hat{\kappa} = 10$), (a) the mobility M, and (b) hydrodynamic effective slip length $\hat{\delta}_{\text{eff}}$, as functions of the phase ϕ, where the solid and dashed lines are respectively for longitudinal and transverse alignment of wall patterns with electric field.

When the wall potentials are constant, the mobilities are enhanced linearly by the corresponding effective slip lengths. As discussed above, the effective slip lengths may

increase or decrease with the phase ϕ, depending on the flow direction. Similar effects of the phase on the mobilities are expected. We show in figure 2 some typical values of $M_{\parallel,\perp}$ and $\hat{\delta}_{\rm eff}^{\parallel,\perp}$ as functions of ϕ, where $\hat{\delta}_0 = 0.5$, 1, $a = 1$ and $b = 0$. Following the trends of the effective slip length, the mobility will decrease for longitudinal flow (solid lines), but will increase for transverse flow (dashed lines), as the phase increases from 0 to π. The longitudinal mobility is, however, always larger than the transverse mobility. The difference is the largest when $\phi = 0$, and the smallest when $\phi = \pi$. Therefore, an in-phase arrangement of the slip patterns is the most anisotropic configuration when the walls are uniformly charged.

3.4 Nonuniform wall potentials

Nonuniform wall potential interacting with nonuniform hydrodynamic slip leads to a much richer behavior. Figure 3 shows that the mobilities may vary in dramatically different trends with the phase ϕ, depending on how the modulation component of the wall potential interacts with the spatially varying wall slip. When they interact positively, $a = b = 1$ as in figure 3(a), for which the peak wall potential meets the peak wall slip, the trends are similar to those shown in figure 2(a) for uniform wall potentials. All the mobility values are amplified. The degree of amplification is the strongest at $\phi = 0$ for the longitudinal flow, and is the strongest at $\phi = \pi$ for the transverse flow. As a result, the contrast between $M_\parallel$ and $M_\perp$ increases at $\phi = 0$, but decreases at $\phi = \pi$. In other words, the effect of positive interaction between wall potential and slip is to enhance flow anisotropy at $\phi = 0$, but to weaken the flow anisotropy at $\phi = \pi$.

When the amplitude of the modulation wall potential is negative, $a = 1$ and $b = -1$ as in figure 3(b), for which the wall potential is zero at the point of maximum slip, while the wall potential is the maximum at the point of zero slip, the mobilities may vary with the phase in a very different manner. As a result of the counter-interaction between wall potential and slip, all the mobility values are diminished. The degree of diminishing turns out to be the strongest at $\phi = 0$ for the longitudinal flow, and the strongest at $\phi = \pi$ for the transverse flow. Consequently, the mobilities change non-monotonically with the phase. As seen in figure 3(b), $M_\parallel$ reaches the minimum and $M_\perp$ reaches the

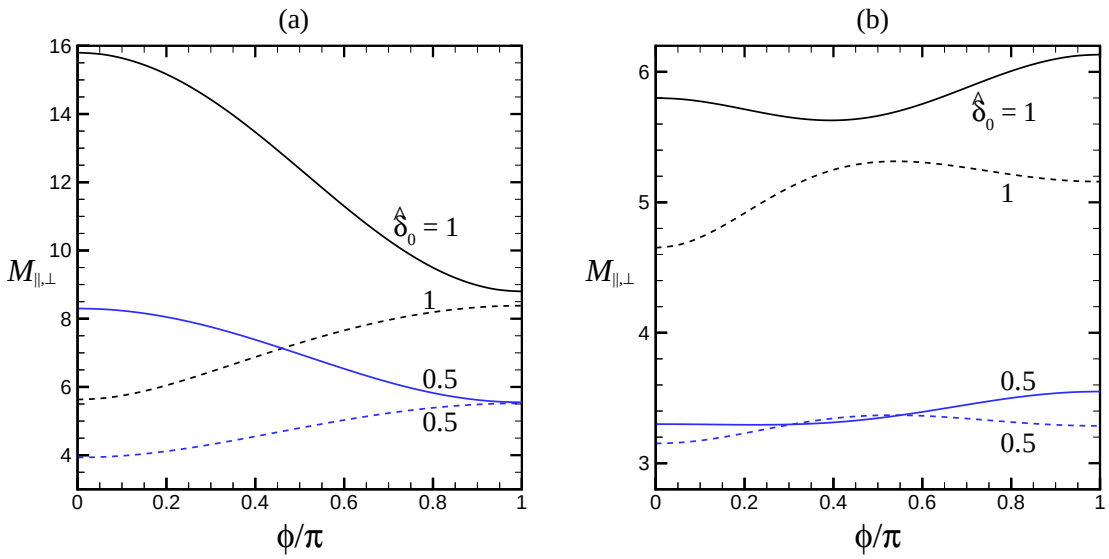

Figure 3: For nonuniformly charged walls ($\hat{\kappa} = 10$), the mobility M as a function of the phase ϕ: (a) $a = 1$, $b = 1$, and (b) $a = 1$, $b = -1$, where the solid and dashed lines are respectively for longitudinal and transverse alignment of wall patterns with electric field.

maximum at a phase in the range $\phi/\pi = 0.4 - 0.5$. In this range, the contrast between $M_\parallel$ and $M_\perp$ is the smallest, and it is even possible that $M_\perp > M_\parallel$ for sufficiently low $\hat{\delta}_0$. Also in sharp contrast to the preceding case, the longitudinal mobility is now the maximum at $\phi = \pi$.

3.5 Negative wall potentials

Let us consider a case in which the wall potential is negative over part of a period. Figure 4 shows $M_{\parallel,\perp}$ as functions of ϕ and $\hat{\delta}_0$, for $a = 0.2$ and $b = -1$. The wall potential is negative (-0.8) at the point of maximum wall slip, and is positive (1.2) at the point of zero wall slip. The average wall potential is positive (0.2). However, it is not necessarily the average wall potential that determines the flow direction. The charge of the more slipping part of the wall tends to outweigh the charge of the less slipping part of the wall in controlling the flow. Here, we see in figure 4(a) that the longitudinal and transverse mobilities are most affected by the charge of the peak slipping region when the two walls are in phase ($\phi = 0$) and half-period out of phase ($\phi = \pi$), respectively. In this case, the negative potential of the peak slipping region is to cause a negative longitudinal

flow at $\phi = 0$, and a negative transverse flow at $\phi = \pi$, despite an average positive wall potential. It is of interest to find that, for sufficiently large $\hat{\delta}_0$, the longitudinal flow is negative but the transverse flow is positive at $\phi = 0$, while the opposite is true at $\phi = \pi$. Flow direction can be reversed by changing the phase of the walls.

It is further shown in figure 4(b) how the mean slip length $\hat{\delta}_0$ may have very different effects on the mobilities at the two limiting phases, $\phi = 0$ and $\phi = \pi$. The contrast between the two mobilities is to increase with increasing $\hat{\delta}_0$ at these two phases. At $\phi = 0$, the trends are mostly linear. When the wall patterns are in phase, the longitudinal flow is more affected by the negatively charged regions of higher slip, while the transverse flow is more subject to the positively charged regions of lower slip. This explains why $M_{\parallel}$ is increasingly negative, while $M_{\perp}$ is increasingly positive, as $\hat{\delta}_0$ increases. This kind of differing behaviors happens when the positive peak charge (associated with lower slip) is moderately larger in magnitude than the negative peak charge (associated with higher slip). At $\phi = \pi$, the trends are nonlinear and non-monotonic. Depending on the mean slip length, the two mobilities can be both positive, both negative, or with opposite signs. These half-period out-of-phase mobilities are in general much smaller in magnitude than their in-phase counterparts.

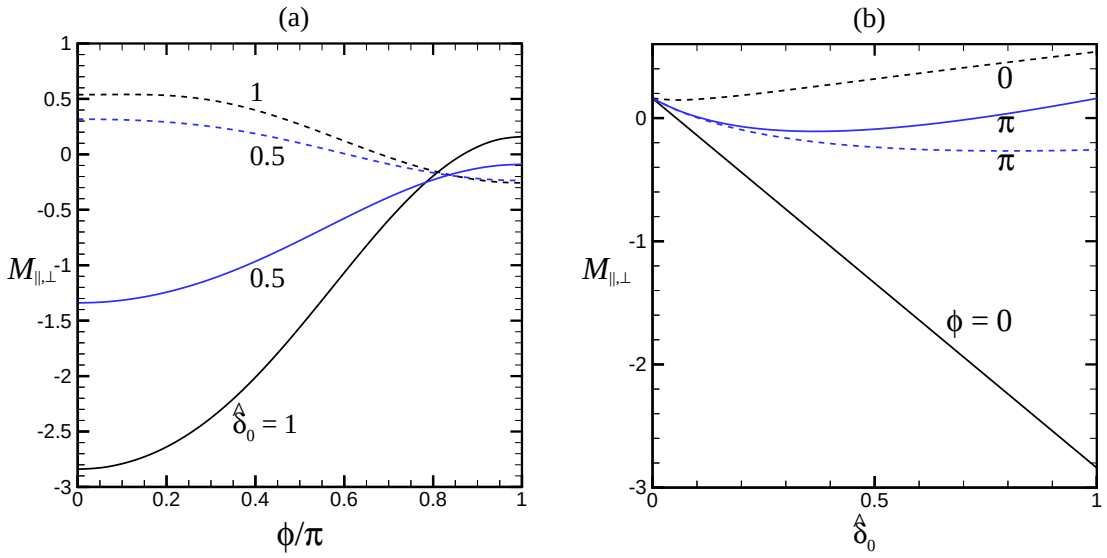

Figure 4: For partly negatively charged walls ($a = 0.2$, $b = -1$, $\hat{\kappa} = 10$), the mobility M as a function of (a) the phase ϕ, and (b) the mean slip length $\hat{\delta}_0$, where the solid and dashed lines are respectively for longitudinal and transverse alignment of wall patterns with electric field.

When the two mobilities are opposite in sign, it is possible to generate a net flow which is in a direction perpendicular to the applied field (Ajdari 1996, 2001). This will happen when $\vec{E} \cdot \vec{V} = 0$ or $M_\perp E_x^2 + M_\parallel E_z^2 = 0$, which determines the specific angle θ with the x-axis at which the field $\vec{E}$ is to be applied to get the transverse effect:

$$\tan^2 \theta = -M_\perp / M_\parallel. \tag{34}$$

3.6 Convection patterns

Lastly, we show in figure 5 some transverse flow patterns, further illustrating the effects of negative wall potential under the in-phase and the half-period out-of-phase conditions. Recall that while the mean flow is due to an externally applied electric field E_x toward the right, the flow is locally affected by pressure gradient which is induced owing to the spatially varying slip lengths and wall potentials. Shown in the figure are streamlines, where the streamfunction is zero on $y = 0$, and is positive (forward flow or counter-clockwise recirculation) and negative (backward flow or clockwise recirculation) when represented by solid and dashed streamlines, respectively. Figure 5(a, b) shows the case $a = 0.2$ and $b = -1.0$, for which, as already discussed above, the net flow is positive when $\phi = 0$, but is negative when $\phi = \pi$. From figure 5(a), we can see that the forward stream encounters high resistance near the wall at $\hat{x} = 0$, where the slip is the largest but the charge is the maximum negative, and also some resistance near the wall at $\hat{x} = 0.5$, where the charge is the maximum positive but the slip is zero. The strong resistance induced by negative wall potential causes recirculation near $\hat{x} = 0$. The flow pattern changes dramatically when the walls are half-period out of phase, as shown in figure 5(b). The backward flow is a relatively thin stream. It goes up and down around convective cells of alternating sense of circulation. The convective cells are large in size and each contains a pair of vortices. The dominance of large convective recirculation in the flow can substantially enhance the mixing efficiency of the flow.

Figure 5(c, d) shows the case $a = 0$ and $b = -1.0$. Although the walls are electro-neutral (i.e. zero average charge), the net flow is always backward in this case. This is because the negative charge, which is associated with the higher slip regions of the walls, will dominate. The backward flow encounters resistance, thereby forming recirculation

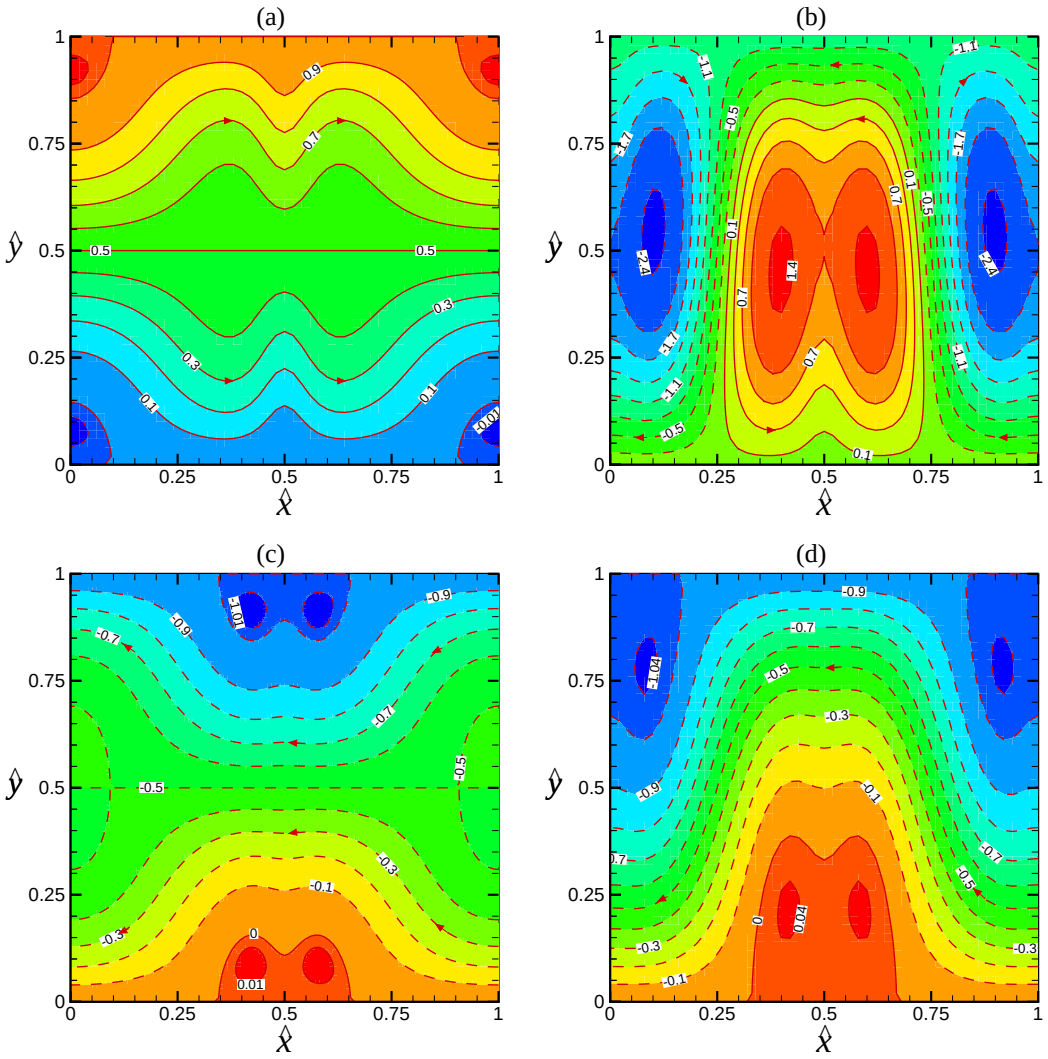

Figure 5: Transverse flow patterns over one wavelength of channel, where solid and dashed lines represent streamlines with positive and negative streamfunction, respectively, ($\hat{\kappa} = 10$, $\hat{\delta}_0 = 1$): (a) $a = 0.2$, $b = -1$, $\phi = 0$, (b) $a = 0.2$, $b = -1$, $\phi = \pi$, (c) $a = 0$, $b = -1$, $\phi = 0$, and (d) $a = 0$, $b = -1$, $\phi = \pi$.

cells, near the positively charged walls. In the in-phase configuration (figure 5(c)), the flow is convergent and confined to the central part of the channel on passing between two such recirculation cells. The flow then divides itself into two divergent streams enclosing a central recirculation zone on passing through the negatively charged walls. This kind of successive convergent and divergent flow behaviors can also be conducive to mixing. In the out-of-phase configuration (figure 5(d)), the backward stream has a sinuous course, meandering upward and downward to go around the regions of high resistance induced by positive wall charge. Convective rolls of alternating direction of circulation are formed in a staggered manner near the two walls. Such a convection pattern can also lead to highly efficient mixing. The flow patterns shown in figure 5(a, c) are somewhat similar to those shown in figure 4 of Belyaev and Vinogradova (2011), who considered EO flow over a striped superhydrophobic surface.

4 Concluding remarks

The superposition of periodic surface charge and hydrodynamic slip patterns can lead to a rich set of behaviors for electro-osmotic (EO) flows. In this paper, we have examined EO flow through a thin channel, using the method of lubrication approximation, for wall patterns varying slowly either in the streamwise or the spanwise direction. It is demonstrated that the phase shift of the wall patterns will have a central role to play in determining not only the section-averaged flow, but also the local secondary flow structure. Depending on the direction of field with respect to the wall modulation, the EO mobility is shown to be a strong function of the phase, exhibiting dramatically different trends as the phase changes.

When mass transport is concerned, the convection is determined by the section-averaged velocity, while the dispersion is determined also by the velocity profile and hence affected by the secondary flow such as recirculation and convective rolls. It is desirable if the present study can be extended to the mass transport problem, with an aim to find out how the dispersion can be controlled (enhanced or suppressed) by a suitable superposition of charge and slip patterns on the channel walls. It is also of interest to relax in the future work some of the assumptions (e.g. linearized Poisson-Boltzmann

equation, non-overlapped electric double layers, slowly varying wall modulation, in-phase slip and potential on the same wall, and so on) in order to broaden the scope of the study.

Acknowledgments

The work was financially supported by the Research Grants Council of the Hong Kong Special Administrative Region, China, through Projects HKU 715609E and HKU 715510E. Comments by the two referees are gratefully acknowledged.

References

Ajdari A 1995 Electro-osmosis on inhomogeneously charged surfaces *Phys. Rev. Lett.* **75** 755–758

Ajdari A 1996 Generation of transverse fluid currents and forces by an electric field: Electro-osmosis on charge-modulated and undulated surfaces *Phys. Rev. E* **53** 4996–5005

Ajdari A 2001 Transverse electrokinetic and microfluidic effects in micropatterned channels: Lubrication analysis for slab geometries *Phys. Rev. E* **65** 016301

Anderson J L and Idol W K 1985 Electroosmosis through pores with nonuniformly charged walls *Chem. Eng. Commum.* **38** 93–106

Belyaev A V and Vinogradova O I 2011 Electro-osmosis on anisotropic superhydrophobic surfaces *Phys. Rev. Lett.* **107** 098301

Chang C C and Yang R J 2007 Electrokinetic mixing in microfluidic systems *Microfluid. Nanofluid.* **3** 501–525

Ghosal S 2002 Lubrication theory for electro-osmotic flow in a microfluidic channel of slowly varying cross-section and wall charge *J. Fluid Mech.* **459** 103–128

Herr A E, Molho J I, Santiago J G, Mungal M G and Kenny T W 2000 Electroosmotic capillary flow with nonuniform zeta potential *Anal. Chem.* **72** 1053–1057

Long D, Stone H A and Ajdari A 1999 Electroosmotic flows created by surface defects in capillary electrophoresis *J. Colloid Interf. Sci.* **212** 338–349

Ng C O and Chu H C W 2011 Electrokinetic flows through a parallel-plate channel with slipping stripes on walls *Phys. Fluids* **23** 102002

Ng C O and Wang C Y 2010 Darcy–Brinkman flow through a corrugated channel *Transp. Porous Med.* **85** 605–618

Squires T M 2008 Electrokinetic flows over inhomogeneously slipping surfaces *Phys. Fluids* **20** 092105

Stroock A D, Weck M, Chiu D T, Huck W T S, Kenis P J A, Ismagilov R F and Whitesides G M 2000 Patterning electro-osmotic flow with patterned surface charge *Phys. Rev. Lett.* **84** 3314–3317

Vinogradova O I and Belyaev A V 2011 Wetting, roughness and flow boundary conditions *J. Phys.: Condens. Matter* **23** 184104

Wang C Y 1976 Parallel flow between corrugated plates *ASCE J. Eng. Mech. Div.* **102** 1088–1090

Wang C Y 1979 On Stokes flow between corrugated plates *ASME J. Appl. Mech.* **46** 462–464